# TranSalNet: Visual saliency prediction using transformers

Jianxun Lou, Hanhe Lin, David Marshall, Dietmar Saupe and Hantao Liu

Abstract—Convolutional neural networks (CNNs) have significantly advanced computational modeling for saliency prediction. However, the inherent inductive biases of convolutional architectures cause insufficient long-range contextual encoding capacity, which potentially makes a saliency model less humanlike. Transformers have shown great potential in encoding long-range information by leveraging the self-attention mechanism. In this paper, we propose a novel saliency model integrating transformer components to CNNs to capture the long-range contextual information. Experimental results show that the new components make improvements, and the proposed model achieves promising results in predicting saliency.

Index Terms—Saliency, deep learning, transformer

## I. Introduction

VISUAL attention mechanism allows humans to select and interpret the most relevant information in the visual scene [1]. Being able to predict saliency is beneficial to various fields including computer vision, robotics, healthcare, and multimedia [2]–[5].

Existing saliency models can be categorized into two classes, traditional and deep learning-based. Traditional models [6]–[8] apply low-level visual features such as color, luminance, texture, and contrast, to simulate the visually salient areas in the scene. These models remain rather limited as higher-level features such as objects are often omitted but they exhibit significant determinants of saliency [9], [10]. Some traditional models [11] have been extended with specific higher-level features, e.g., faces and texts, there are still obstacles in combining low- and higher-level visual features.

Rather than designing handcrafted features, deep learning-based saliency models automatically discover representations from images. eDN [12] represents one of the first models that adopted shallow convolutional neural networks (CNNs) to detect visual saliency of natural images. DeepGaze and DeepGaze II [13], which were based on AlexNet [14] and VGG-19 [15], respectively, successfully built pre-trained networks as feature extractors to train deeper networks for

Jianxun Lou, David Marshall, and Hantao Liu are with the School of Computer Science and Informatics, Cardiff University, Cardiff, United Kingdom. Hanhe Lin is with the National Subsea Centre, Robert Gordon University, AB10 7AQ Aberdeen, United Kingdom.

Dietmar Saupe is with the Department of Computer and Information Science, University of Konstanz, 78464 Konstanz, Germany.

Funded in part by the Deutsche Forschungsgemeinschaft (DFG, German Research Foundation) – Project-ID 251654672 – TRR 161.

© 20xx IEEE. Personal use of this material is permitted. Permission from IEEE must be obtained for all other uses, in any current or future media, including reprinting/republishing this material for advertising or promotional purposes, creating new collective works, for resale or redistribution to servers or lists, or reuse of any copyrighted component of this work in other works.

saliency prediction. By comparing VGG-16 [15], AlexNet, and GoogleNet [16], Huang et al. [17] found that VGG-16 detects saliency more effectively than the other two models, and proposed a CNN-based model to obtain saliency semantic objects with different granularities. ML-Net [18] adopted skip-connections to concatenate feature maps from different layers and set learnable Gaussian parameters for center prior modeling. In order to obtain multi-scale contextual information, Wang et al. [19] used an encoder-decoder with skip architecture CNNs to detect saliency by utilizing features of three different scales. Similarly, MSI-NET [20] used a skip architecture to first extract multi-scale features from dilated convolution and then fuse them by Atrous Spatial Pyramid Pooling [21]. Cornia et al. [22] developed saliency models that simulate the attention mechanism using a Long-Short Term Memory (LSTM)-based architecture. It also demonstrated that ResNet [23] is a high performance feature extraction network for saliency prediction.

Despite the above significant progress, each convolution kernel in CNNs only receives information from a local subset of pixels in an image, which makes CNN-based models deficient in obtaining long-range and global contextual information. Previous research attempted to solve this problem by either capturing multi-scale information [17]–[20], or using network structures with long-range modeling capabilities to increase spatial representations [22].

The transformer [24], which consists of a self-attention mechanism, provides an elegant solution to the above problem. By effectively modeling long-range dependency, the transformer has proven efficacy in the field of natural language processing [25] and more recently achieved promising results in computer vision tasks [26], [27]. However, the use of transformers in visual saliency prediction has not been explored until now.

In this article, we propose a novel saliency prediction model, namely TranSalNet, that integrates transformers and CNNs. We demonstrate the benefits of transformer components in saliency prediction.

# II. THE PROPOSED MODEL

The overview of our proposed TranSalNet model is shown in Fig. 1. A given image is fed into a CNN encoder, i.e., ResNet-50 [23], where three sets of feature maps are extracted from different convolutional blocks. These feature maps are passed through three transformer encoders, yielding contextenhanced feature maps. The CNN decoder fuses these feature maps for saliency prediction.

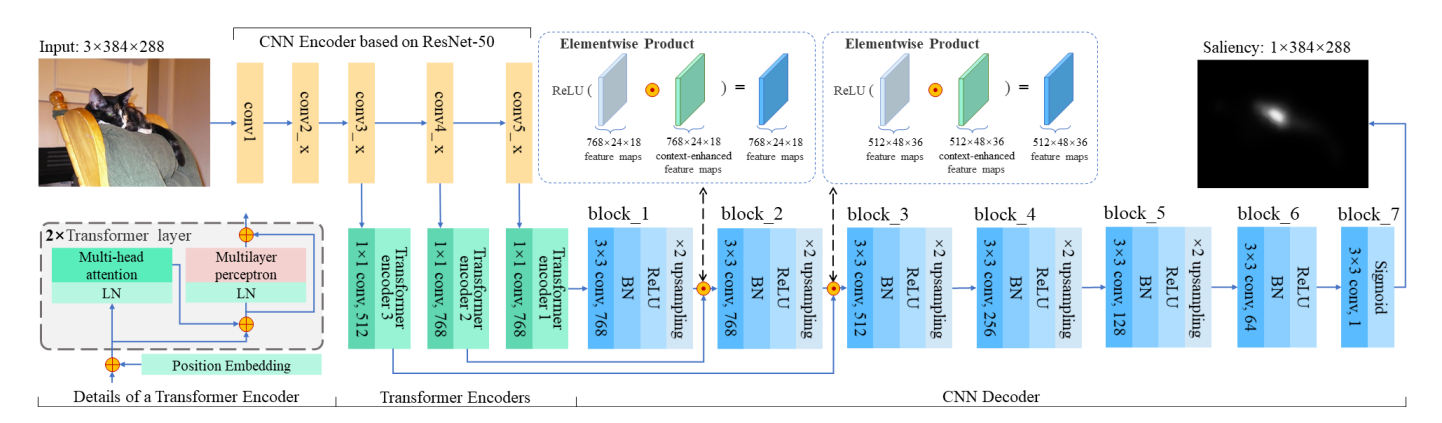


Fig. 1. Overview of TranSalNet. After the input image is processed by the CNN encoder based on ResNet-50, three sets of multi-scale feature maps are obtained from conv5\_x, conv4\_x, and conv3\_x. Then the contextual information of these feature maps is enhanced by transformer encoders. The predicted saliency map is generated by the CNN decoder, which uses skip-connection and element-wise production to fuse multi-scale context-enhance feature maps. The illustration of the transformer encoder based on the Vision Transformer [26], which is shown at the bottom left of the figure.

#### A. The CNN encoder

The CNN encoder corresponds to the ResNet-50 CNN body with weights pre-trained on ImageNet [28]. It is composed of five convolutional blocks that are denoted as conv1 and conv2\_x to conv5\_x. Although previous work [17]–[20] showed that adopting multi-scale feature maps is beneficial to saliency prediction, our experiments found that using feature maps from shallower network blocks, i.e. the conv1 and conv2\_x, may cause borderlines and artifacts to appear incorrectly in the saliency maps. Therefore, we extracted feature maps from the deeper conv3\_x, conv4\_x, and conv5\_x blocks.

## B. The transformer encoder

The three sets of multi-scale feature maps are respectively fed into three transformer encoders to enhance the long-range and contextual information. The details of transformer are depicted at the bottom left of Fig. 1. Let  $\mathbf{x}_1$ ,  $\mathbf{x}_2$ , and  $\mathbf{x}_3$  be the feature maps that are extracted from the conv5\_x, conv4\_x, and conv3\_x blocks respectively. First, a  $1 \times 1$  convolution layer ( $Conv_{1\times 1}$ ) is used to reduce the computational cost and align with the acceptable input size of the transformer encoder. Specifically,  $\mathbf{x}_1$  and  $\mathbf{x}_2$  are reduced from 2048 and 1024 dimensions to 768 dimensions, and  $\mathbf{x}_3$  remains unchanged at 512 dimensions. As there is no relative or absolute position information in the feature maps, position embedding (POS) that uses element-wise addition of input and a trainable matrix is operated before feeding it into the transformer encoders. Each transformer encoder contains two same layers of Multihead Self-Attention (MSA) and Multi-layer Perceptron (MLP) blocks. In our model, we applied 12-heads attention in transformer encoder 1 and 2, and 8-heads in encoder 3. The MLP block contains two layers with a GELU activation function. Besides, Layer Normalization (LN) and residual connection are applied before and after each block respectively. The processing in each transformer encoder can be represented as:

$$\mathbf{z}_0 = \operatorname{Conv}_{1 \times 1}(\mathbf{x}_i) \oplus \operatorname{POS}_i, \ i = 1, 2, 3 \tag{1}$$

$$\mathbf{z}_{l}^{'} = MSA(LN(\mathbf{z}_{l-1})) \oplus \mathbf{z}_{l-1}, \ l = 1, 2$$
 (2)

$$\mathbf{z}_{l} = \text{MLP}(\text{LN}(\mathbf{z}_{l}^{'})) \oplus \mathbf{z}_{l}^{'}, \ l = 1, 2 \tag{3}$$

where  $\mathbf{z}_l$  is the output feature map of the l-th layer in transformer encoder, and  $\mathbf{x}_i$  is the input feature map from the CNN encoder. The feature maps that are passed through transformer encoder 1, 2, and 3 are context-enhanced and denoted as  $\mathbf{x}_1^c$ ,  $\mathbf{x}_2^c$ , and  $\mathbf{x}_3^c$  respectively. The computation of transformer is detailed in [26].

## C. The CNN decoder

The CNN decoder is a fully CNN network containing block\_1 to block\_7, which is used to implement pixel-level classification to predict saliency maps. Batch normalization (BN) and the activation function (ReLU for block\_1 to block\_6; Sigmoid for block\_7) are applied after each  $3 \times 3$ convolution operation ( $Conv_{3\times3}$ ), where the former was used to promote the convergence and the latter was used to increase the nonlinear factor of the model. Since the input image is 32scale downscaled by the encoder network, a 2-scale upsampling that adopts nearest-neighbor interpolation is performed to the feature map in block\_1 to block\_5 to obtain a saliency map of the same size as the input. In order to enhance the long-range and multi-scale context of the feature map during the decoding process, the upsampled feature map and the transformer's output from the corresponding skip-connection are fused by an element-wise product operation. The processes from block\_1 to block\_6 can be expressed as:

$$\mathbf{x}_{i}^{f} = \begin{cases} \mathbf{x}_{i}^{c}, & i = 1 \\ \text{ReLU}(\text{Upsample}(\hat{\mathbf{x}}_{i-1}^{f}) \odot \mathbf{x}_{i}^{c}), & i = 2, 3 \\ \text{Upsample}(\hat{\mathbf{x}}_{i-1}^{f}), & i = 4, 5, 6 \end{cases} \tag{4}$$

$$\hat{\mathbf{x}}_{i}^{f} = \text{ReLU}(\text{BN}(\text{Conv}_{3\times3}(\mathbf{x}_{i}^{f}))), \ i = 1, 2, \dots, 6$$
 (7)

where  $\mathbf{x}_i^f$  and  $\hat{\mathbf{x}}_i^f$  are the input and output features of the *i*-th block. The output block, i.e., block\_7, is used to reduce the dimensionality of the feature map to a 2D map for pixel-level classification. Therefore, the sigmoid activation function is applied to the feature map:

$$\hat{\mathbf{y}} = \operatorname{sigmoid}(\operatorname{Conv}_{3\times3}(\hat{\mathbf{x}}_6^f)),\tag{8}$$

where  $\hat{\mathbf{y}}$  is the predicted saliency map.

## D. Loss function

Recent saliency prediction studies [22], [29], [30] have shown that taking advantage of the saliency evaluation metrics to define the loss function can significantly improve the performance of saliency prediction models.

Following a similar idea, we adopted a linear combination of four metrics as the loss function to train our model, including the Normalized Scanpath Saliency (NSS), Kullback-Leibler divergence (KLD), Linear Correlation Coefficient (CC), and Similarity (SIM). Let  $\mathbf{y}^s$ ,  $\mathbf{y}^f$ , and  $\hat{\mathbf{y}}$  be the ground truth saliency map, fixation map, and predicted saliency map, and i indicates the ith pixel of  $\mathbf{y}^s$  and  $\hat{\mathbf{y}}$ , our loss function is defined as:

$$L(\mathbf{y}^{s}, \mathbf{y}^{f}, \hat{\mathbf{y}}) = \lambda_{1} L_{\text{NSS}}(\mathbf{y}^{f}, \hat{\mathbf{y}}) + \lambda_{2} L_{\text{KLD}}(\mathbf{y}^{s}, \hat{\mathbf{y}}) + \lambda_{3} L_{\text{CC}}(\mathbf{y}^{s}, \hat{\mathbf{y}}) + \lambda_{4} L_{\text{SIM}}(\mathbf{y}^{s}, \hat{\mathbf{y}}),$$

$$(9)$$

where  $\lambda_1$ ,  $\lambda_2$ ,  $\lambda_3$ , and  $\lambda_4$  are the weights of each metric, and

$$L_{\text{NSS}}(\mathbf{y}^f, \hat{\mathbf{y}}) = \frac{1}{\sum_i \mathbf{y}_i^f} \sum_i \frac{\hat{\mathbf{y}}_i - \mu(\hat{\mathbf{y}})}{\sigma(\hat{\mathbf{y}})} \mathbf{y}_i^f, \tag{10}$$

where  $\sigma(\cdot)$  and  $\mu(\cdot)$  stand for standard deviation and mean respectively;

$$L_{\text{KLD}}(\mathbf{y}^s, \hat{\mathbf{y}}) = \sum_{i} \mathbf{y}_i^s \log(\epsilon + \frac{\mathbf{y}_i^s}{\epsilon + \hat{\mathbf{y}}_i}), \tag{11}$$

where  $\epsilon$  is a regularization constant and set to  $2.2204 \times 10^{-16}$ ;

$$L_{\text{CC}}(\mathbf{y}^s, \hat{\mathbf{y}}) = \frac{\text{cov}(\mathbf{y}^s, \hat{\mathbf{y}})}{\sigma(\mathbf{v}^s)\sigma(\hat{\mathbf{y}})},$$
(12)

where  $cov(\cdot)$  is the covariance and  $\sigma(\cdot)$  is standard deviation;

$$L_{\text{SIM}}(\mathbf{y}^s, \hat{\mathbf{y}}) = \sum_{i} \min(\mathbf{y}_i^s, \hat{\mathbf{y}}_i). \tag{13}$$

In  $L_{\text{KLD}}$ ,  $L_{\text{CC}}$  and  $L_{\text{SIM}}$ ,  $\mathbf{y}^s$ , and  $\hat{\mathbf{y}}$  are normalized so that  $\sum_i \mathbf{y}_i^s = \sum_i \hat{\mathbf{y}}_i = 1$ . According to our empirical studies, the weights  $\lambda_1$ ,  $\lambda_2$ ,  $\lambda_3$ , and  $\lambda_4$  of the combined loss function are set to -1, 10, -2, and -1 respectively for balancing each sub-loss impact.

# III. EXPERIMENTAL RESULTS

# A. Datasets

Four commonly used benchmark saliency datasets were used to train and evaluate our proposed saliency model.

- SALICON [31] contains 10,000 training and 5,000 validation images. Different from other benchmark datasets, it employs mouse clicks instead of an eye tracker to record human attention.
- CAT2000 [32] contains 2,000 publicly released images of 20 categories such as action, art, cartoon etc, where each category includes 100 images. Each image has eyetracking data of 24 observers.
- MIT1003 [33] consists of 1,003 natural indoor and outdoor images with eye-tracking data of 15 observers.
- MIT300 [34] has 300 natural indoor and outdoor images.
   The eye-tracking data is unpublished, it is used as the test set of the MIT/Tübingen benchmark [35].

# B. Setup

By following a similar procedure in the state-of-the-art [13], [17], [19], [20], [22], a model was first pre-trained on the 10,000 images of the SALICON training set to reduce the risk of overfitting, then the best model on its validation set was selected for further training on MIT1003 and CAT2000. To obtain fair results in each dataset, k-fold cross-validation (k = 10) was applied for each model. More specifically, each dataset was divided into 10 non-overlapping subsets. For MIT1003, each subset contains around 100 images; For CAT2000, each subset contains 200 images (10 from each category). Each time, one subset was kept as a test set, one as a validation set, and the remaining eight subsets were used as the training set. To eliminate randomness, each test set corresponds to a fixed validation set and training set. We report the overall performance of 10 times test results. To reduce the computational cost while aligning with the aspect ratio (4:3) of the images in SALICON, all input images were resized and padded to a same size of 384×288 px. During the training phase, the Adam optimizer [36] was used to minimize the loss function. The training rate was set to  $1 \times 10^{-5}$ , which was then multiplied by 0.1 every 3 epochs. Models were trained with a batch size of 4 for 30 epochs with a stop patience of 5 epochs.

# C. Ablation study

Ablation experiments were conducted to investigate the contribution of the skip-connection, transformer encoder, and combined loss function. To this end four model variants were constructed as follows.

- BaseNet: Compared with TranSalNet, it removes all transformer encoders and skip-connections except for the Conv<sub>1×1</sub> layer before transformer encoder 1. The binary cross entropy (BCE) loss was used.
- BaseNet+: It adds only one transformer module, i.e., transformer encoder 1, on the basis of BaseNet. BCE loss was used.
- 3) SkipNet: It is similar to the BaseNet, but with two skip-connections and Conv<sub>1×1</sub> layers added. In other words, it is equivalent to the proposed TranSalNet model without all transformer encoders. BCE loss was used.
- 4) **TranSalNet\_BCE**: The proposed TranSalNet model but with the BCE loss.
- 5) **TranSalNet**: The proposed TranSalNet model that adopts the combined loss function.

The performance of a saliency model is often quantified by six popular metrics, including NSS, KLD, CC, SIM, AUC (Area under ROC Curve) and sAUC (Shuffled AUC). Detail of these metrics can be found in [39]. Good saliency models should have high values for NSS, CC, SIM, AUC and sAUC, and low values for KLD. The performance of the four model variants is shown in Table I. By comparing BaseNet and BaseNet+, adding a transformer encoder can improve the performance of the model in all metrics except for KLD on MIT1003 and sAUC on CAT2000. Besides, by adding skip-connections, SkipNet improves on all metrics except for the AUC for MIT1003 and the SIM for both datasets. In general, the above results show that adding transformer and

TABLE I RESULTS OF ABLATION STUDIES ON  $\bf MIT1003$  and  $\bf CAT2000$ 

	MIT1003						CAT2000					
MODEL	sAUC ↑	AUC ↑	NSS ↑	CC ↑	SIM ↑	$KLD \downarrow$	sAUC ↑	AUC ↑	NSS ↑	CC ↑	SIM ↑	$KLD \downarrow$
BaseNet	0.7460	0.9018	2.7129	0.7361	0.5858	0.7886	0.6062	0.8775	2.3043	0.8536	0.7277	0.5190
BaseNet+	0.7472	0.9046	2.7437	0.7446	0.6003	0.8369	0.6054	0.8784	2.3286	0.8622	0.7343	0.5056
SkipNet	0.7505	0.9011	2.7571	0.7393	0.5381	0.7327	0.6111	0.8782	2.3298	0.8582	0.7187	0.3207
TranSalNet_BCE	0.7507	0.9086	2.8326	0.7593	0.6122	0.7785	0.6035	0.8803	2.3887	0.8765	0.7458	0.5040
TranSalNet	0.7546	0.9093	2.8501	0.7595	0.6145	0.7779	0.6054	0.8811	2.4154	0.8786	0.7492	0.5036

TABLE II
PERFORMANCE COMPARISON ON MIT1003 AND CAT2000. RED AND ORANGE FONT INDICATE THE BEST AND 2ND BEST SCORE, RESPECTIVELY.

	MIT1003						CAT2000					
MODEL	sAUC ↑	AUC ↑	NSS ↑	CC ↑	SIM ↑	$KLD \downarrow$	sAUC ↑	AUC ↑	NSS ↑	CC ↑	SIM ↑	$KLD \downarrow$
MSI-NET	0.7454	0.9068	2.8007	0.7473	0.6081	0.8155	0.6071	0.8809	2.3547	0.8655	0.7398	0.4280
SAM-VGG	0.7256	0.9003	2.7520	0.7260	0.5976	1.2195	0.5966	0.8784	2.4138	0.8680	0.7391	0.6383
SAM-ResNet	0.7365	0.9024	2.8001	0.7466	0.6068	1.2470	0.5932	0.8778	2.4108	0.8706	0.7395	0.6702
ML-Net	0.7218	0.8623	2.3329	0.5979	0.4960	1.3496	0.6212	0.8104	1.4485	0.5221	0.5407	1.1101
DVA	0.7359	0.8995	2.6483	0.7105	0.5525	0.7229	0.6098	0.8757	2.1698	0.8110	0.7020	0.4123
TranSalNet	0.7546	0.9093	2.8501	0.7595	0.6145	0.7779	0.6054	0.8811	2.4154	0.8786	0.7492	0.5036

TABLE III

COMPARISON RESULTS OF SALIENCY MODELS ON MIT300. THE RESULTS ARE ADMINISTERED AND REPORTED BY THE BENCHMARK [35]. RED AND ORANGE FONT INDICATE THE BEST AND 2ND BEST SCORE, RESPECTIVELY.

MODEL	sAUC ↑	AUC ↑	NSS ↑	CC ↑	SIM ↑	KLD ↓
EML-NET [29]	0.7469	0.8762	2.4876	0.7893	0.6756	0.8439
CASNet II [37]	0.7398	0.8552	1.9859	0.7054	0.5806	0.5857
GazeGAN [30]	0.7316	0.8607	2.2118	0.7579	0.6491	1.3390
SAM-VGG [22]	0.7305	0.8473	1.9552	0.6630	0.5986	1.2746
SAM-ResNet [22]	0.7396	0.8526	2.0628	0.6897	0.6122	1.1710
DVA [19]	0.7257	0.8430	1.9305	0.6631	0.5848	0.6293
ML-Net [18]	0.7399	0.8386	1.9748	0.6633	0.5819	0.8006
eDN [12]	0.6180	0.8171	1.1399	0.4518	0.4112	1.1369
SalGAN [38]	0.7354	0.8498	1.8620	0.6740	0.5932	0.7574
TranSalNet	0.7471	0.8730	2.3758	0.7991	0.6852	0.9019

skip-connection components are both effective to improve saliency prediction. By uniting transformer encoders and skip-connections, the model performance (see TranSalNet\_BCE) is further boosted on most metrics compared to the previous variants. By comparing TranSalNet\_BCE with TranSalNet, it shows that the combined loss outperforms the BCE loss on all metrics in MIT1003 and in CAT2000.

# D. Comparison with state-of-the-art methods

Five deep learning-based saliency models that adopt skip-connections or attention mechanisms, including MSI-Net, SAM-VGG, SAM-ResNet, ML-NET, and Deep Visual Attention (DVA) were selected for the performance comparison on the MIT1003 and CAT2000. To ensure a fair comparison, the same k-fold Cross-Validation (k=10) strategy and the datasets splitting method used in TranSalNet were employed for fine-tuning and testing of these models. The corresponding pre-trained weights on the SALICON data set was loaded for each fine-tuning instance. Similarly, the overall performance of 10 times test results is reported in Table II. It can be seen that our model achieves best or 2nd best scores on all metrics in MIT1003 and all metrics except for sAUC in CAT2000.

For the MIT300 dataset, we used the MIT1003 to train an optimal model, in which 703 images were randomly selected

as a training set and the rest as a validation set. The optimal model was submitted to and tested by the MIT/Tuebingen Saliency Benchmark [35]. It should be noted that the benchmark evaluates models by different standards, i.e., models must be explicitly claimed as either probabilistic or nonprobabilistic models, so they can be fairly evaluated within the category they belong to [39]. In this paper, same as the original MIT Saliency Benchmark [39], we "do not assume that our model is probabilistic". Note that for evaluating probabilistic models, metric-specific adaptations are applied using regularization and scaling of saliency values, hence, a probabilistic model generates optimal saliency maps for individual metrics [40]. But a non-probabilistic model only outputs a single saliency map for all metrics. So it is nontrivial to compare a non-probabilistic model to a probabilistic model [39]. To avoid unfairly model comparison under different assumptions, Table III shows only non-probabilistic saliency models on the leaderboard of [35]. It can be seen that our model consistently ranks in the top 2 on all metrics except for KLD. In addition, even though we include top probabilistic models such as DeepGaze II-E [41], MSI-NET [20], UNISAL [42], and DeepGaze II [13] for performance comparison, our model can still keep the top 2 places in CC and SIM (results available on website of [35]).

It is crucial to note that metric selection for saliency model evaluation should be based on specific modeling assumptions and specific target applications [39]. The study in [39] concludes that "under the assumptions of non-probabilistic modeling, NSS and CC provide the fairest comparison". If "evaluating probabilistic models, KLD is recommended". "Specific tasks and applications also call for a difference choice of metrics", e.g., CC and SIM are the most appropriate saliency evaluation metrics for image quality assessment applications [43]; and "CC and SIM best correspond to human perception" [44]. Therefore, the proposed saliency model could be the best "human-like" model (i.e., based on perception-based metrics CC and SIM) to evaluate the relative importance of different image regions for the applications such as image re-targeting, image compression and transmission, and visual

quality assessment.

#### IV. CONCLUSION

In this paper, we have proposed a novel saliency model integrating transformers with CNNs. An ablation study has demonstrated the contributions of the new components of the model. Experimental results show that the proposed model achieves promising performance and has the potential to advance many image processing applications.

## REFERENCES

- [1] J. Jonides, D. Irwin, and S. Yantis, "Integrating visual information from successive fixations," *Sci.*, vol. 215, no. 4529, pp. 192–194, 1982.
- [2] A. Borji, "Saliency prediction in the deep learning era: Successes and limitations," *IEEE Trans. Pattern Anal. Mach. Intell.*, vol. 43, no. 2, p. 679—700, February 2021.
- [3] W. Zhang, R. R. Martin, and H. Liu, "A saliency dispersion measure for improving saliency-based image quality metrics," *IEEE Trans. Circuits Syst. Video Technol.*, vol. 28, no. 6, pp. 1462–1466, 2018.
- [4] M. Paul and M. Musfequs Salehin, "Spatial and motion saliency prediction method using eye tracker data for video summarization," *IEEE Trans. Circuits Syst. Video Technol.*, vol. 29, no. 6, pp. 1856–1867, 2019.
- [5] K. Gu, G. Zhai, X. Yang, W. Zhang, and C. W. Chen, "Automatic contrast enhancement technology with saliency preservation," *IEEE Trans. Circuits Syst. Video Technol.*, vol. 25, no. 9, pp. 1480–1494, 2015.
- [6] D. Walther and C. Koch, "Modeling attention to salient proto-objects," Neural Networks, vol. 19, no. 9, pp. 1395–1407, 2006.
- [7] J. Harel, C. Koch, and P. Perona, "Graph-based visual saliency," in Proc. of the 19th Int. Conf. on Neural Inf. Process. Syst., ser. NIPS'06. Cambridge, MA, USA: MIT Press, 2006, p. 545–552.
- [8] E. Erdem and A. Erdem, "Visual saliency estimation by nonlinearly integrating features using region covariances," *J. of Vision*, vol. 13, no. 4, pp. 11–11, 03 2013. [Online]. Available: https://doi.org/10.1167/13.4.11
- [9] J. Stoll, M. Thrun, A. Nuthmann, and W. Einhäuser, "Overt attention in natural scenes: Objects dominate features," *Vision Res.*, vol. 107, pp. 36–48, 2015.
- [10] W. Einhäuser, M. Spain, and P. Perona, "Objects predict fixations better than early saliency," *J. of Vision*, vol. 8, no. 14, pp. 18–18, 11 2008.
- [11] M. Cerf, E. P. Frady, and C. Koch, "Faces and text attract gaze independent of the task: Experimental data and computer model," *J.* of Vision, vol. 9, no. 12, pp. 10–10, 11 2009.
- [12] E. Vig, M. Dorr, and D. Cox, "Large-scale optimization of hierarchical features for saliency prediction in natural images," in 2014 IEEE Conf. on Comput. Vision and Pattern Recognit., 2014, pp. 2798–2805.
- [13] M. Kummerer, T. S. A. Wallis, L. A. Gatys, and M. Bethge, "Understanding low- and high-level contributions to fixation prediction," in *Proc. of the IEEE Int. Conf. on Comput. Vision (ICCV)*, Oct 2017.
- [14] A. Krizhevsky, I. Sutskever, and G. Hinton, "Imagenet classification with deep convolutional neural networks," *Neural Inf. Process. Syst.*, vol. 25, 01 2012.
- [15] K. Simonyan and A. Zisserman, "Very deep convolutional networks for large-scale image recognition," in *Int. Conf. on Learn. Represent.*, 2015.
- [16] C. Szegedy, W. Liu, Y. Jia, P. Sermanet, S. Reed, D. Anguelov, D. Erhan, V. Vanhoucke, and A. Rabinovich, "Going deeper with convolutions," in 2015 IEEE Conf. on Comput. Vision and Pattern Recognit. (CVPR), 2015, pp. 1–9.
- [17] X. Huang, C. Shen, X. Boix, and Q. Zhao, "SALICON: Reducing the semantic gap in saliency prediction by adapting deep neural networks," in 2015 IEEE Int. Conf. on Comput. Vision (ICCV), 2015, pp. 262–270.
- [18] M. Cornia, L. Baraldi, G. Serra, and R. Cucchiara, "A deep multi-level network for saliency prediction," in 2016 23rd Int. Conf. on Pattern Recognit. (ICPR), 2016, pp. 3488–3493.
- [19] W. Wang and J. Shen, "Deep visual attention prediction," *IEEE Trans. Image Process.*, vol. 27, no. 5, pp. 2368–2378, 2018.
- [20] A. Kroner, M. Senden, K. Driessens, and R. Goebel, "Contextual encoder–decoder network for visual saliency prediction," *Neural Networks*, vol. 129, pp. 261–270, 2020.
- [21] L. Chen, G. Papandreou, I. Kokkinos, K. Murphy, and A. L. Yuille, "DeepLab: Semantic image segmentation with deep convolutional nets, atrous convolution, and fully connected CRFs," *IEEE Trans. Pattern Anal. Mach. Intell.*, vol. 40, no. 4, pp. 834–848, 2018.

- [22] M. Cornia, L. Baraldi, G. Serra, and R. Cucchiara, "Predicting human eye fixations via an LSTM-based saliency attentive model," *IEEE Trans. Image Process.*, vol. 27, no. 10, pp. 5142–5154, 2018.
- [23] K. He, X. Zhang, S. Ren, and J. Sun, "Deep residual learning for image recognition," in 2016 IEEE Conf. on Comput. Vision and Pattern Recognit. (CVPR), 2016, pp. 770–778.
- [24] A. Vaswani, N. Shazeer, N. Parmar et al., "Attention is all you need," in Advances in Neural Inf. Process. Syst., I. Guyon, U. V. Luxburg, S. Bengio et al., Eds., vol. 30. Curran Associates, Inc., 2017.
- [25] J. Devlin, M.-W. Chang, K. Lee, and K. Toutanova, "BERT: Pretraining of deep bidirectional transformers for language understanding," in Proc. of the 2019 Conf. of the North Amer. Chapter of the Assoc. for Comput. Linguistics: Human Lang. Technol., Volume 1 (Long and Short Papers). Minneapolis, Minnesota: Association for Computational Linguistics, Jun. 2019, pp. 4171–4186.
- [26] A. Dosovitskiy, L. Beyer, A. Kolesnikov et al., "An image is worth 16x16 words: Transformers for image recognition at scale," in *Int. Conf.* on Learn. Represent., 2021.
- [27] M. Chen, A. Radford, R. Child et al., "Generative pretraining from pixels," in Proc. of the 37th Int. Conf. on Mach. Learn., ser. Proc. of Machine Learning Research, H. D. III and A. Singh, Eds., vol. 119. PMLR, 13–18 Jul 2020, pp. 1691–1703. [Online]. Available: http://proceedings.mlr.press/v119/chen20s.html
- [28] O. Russakovsky, J. Deng, H. Su, J. Krause, S. Satheesh, S. Ma, Z. Huang, A. Karpathy, A. Khosla, M. Bernstein, A. C. Berg, and L. Fei-Fei, "ImageNet Large Scale Visual Recognition Challenge," *Int. J. of Comput. Vision (IJCV)*, vol. 115, no. 3, pp. 211–252, 2015.
- [29] S. Jia and N. D. Bruce, "EML-NET: An expandable multi-layer network for saliency prediction," *Image and Vision Comput.*, vol. 95, p. 103887, 2020.
- [30] Z. Che, A. Borji, G. Zhai, X. Min, G. Guo, and P. Le Callet, "How is gaze influenced by image transformations? Dataset and model," *IEEE Trans. Image Process.*, vol. 29, pp. 2287–2300, 2020.
- [31] M. Jiang, S. Huang, J. Duan, and Q. Zhao, "SALICON: Saliency in context," in 2015 IEEE Conf. on Comput. Vision and Pattern Recognit. (CVPR), 2015, pp. 1072–1080.
- [32] A. Borji and L. Itti, "CAT2000: A large scale fixation dataset for boosting saliency research," CVPR 2015 workshop on "Future of Datasets", 2015, arXiv preprint arXiv:1505.03581.
- [33] T. Judd, K. Ehinger, F. Durand, and A. Torralba, "Learning to predict where humans look," in 2009 IEEE 12th Int. Conf. on Comput. Vision, 2009, pp. 2106–2113.
- [34] T. Judd, F. Durand, and A. Torralba, "A benchmark of computational models of saliency to predict human fixations," MIT Computer Science and Artificial Intelligence Lab (CSAIL), Cambridge, MA, USA, Tech. Rep. MIT-CSAIL-TR-2012-001, 01 2012.
- [35] M. Kümmerer, Z. Bylinskii, T. Judd, A. Borji, L. Itti, F. Durand, A. Oliva, and A. Torralba, "MIT/Tübingen Saliency Benchmark," https://saliency.tuebingen.ai/.
- [36] D. P. Kingma and J. Ba, "Adam: A method for stochastic optimization," arXiv preprint arXiv:1412.6980, 2014.
- [37] S. Fan, Z. Shen, M. Jiang, B. L. Koenig, J. Xu, M. S. Kankanhalli, and Q. Zhao, "Emotional attention: A study of image sentiment and visual attention," in 2018 IEEE Conf. on Comput. Vis. and Pattern Recognit. (CVPR), June 2018.
- [38] J. Pan, C. Canton, K. McGuinness, N. E. O'Connor, J. Torres, E. Sayrol, and X. a. Giro-i Nieto, "Salgan: Visual saliency prediction with generative adversarial networks," in arXiv, January 2017.
- [39] Z. Bylinskii, T. Judd, A. Oliva, A. Torralba, and F. Durand, "What do different evaluation metrics tell us about saliency models?" *IEEE Trans. Pattern Anal. Mach. Intell.*, vol. 41, no. 3, pp. 740–757, 2019.
- [40] M. Kummerer, T. S. A. Wallis, and M. Bethge, "Saliency benchmarking made easy: Separating models, maps and metrics," in *Proc. Eur. Conf. Comput. Vis.* (ECCV), September 2018, pp. 770–787.
- [41] L. Akis, K. Matthias, P. Ori, and B. Matthias, "Deepgaze iie: Calibrated prediction in and out-of-domain for state-of-the-art saliency modeling," in arXiv, September 2021.
- [42] R. Droste, J. Jiao, and J. A. Noble, "Unified Image and Video Saliency Modeling," in Proc. of the 16th Eur. Conf. on Comput. Vis. (ECCV), 2020.
- [43] X. Yang, F. Li, and H. Liu, "A measurement for distortion induced saliency variation in natural images," *IEEE Trans. on Instrum. Meas.*, vol. 70, pp. 1–14, 2021.
- [44] J. Li, C. Xia, Y. Song, S. Fang, and X. Chen, "A data-driven metric for comprehensive evaluation of saliency models," in 2015 IEEE Int. Conf. on Comput. Vision (ICCV), Dec 2015, pp. 190–198.